

# Time–frequency transform approach for protection of parallel transmission lines

P.K. Dash, S.R. Samantaray, G. Panda and B.K. Panigrahi

**Abstract:** A new approach for protection of parallel transmission lines is presented using a time–frequency transform known as the *S*-transform that generates the *S*-matrix during fault conditions. The *S*-transform is an extension of the wavelet transform and provides excellent time localisation of voltage and current signals during fault conditions. The change in energy is calculated from the *S*-matrix of the current signal using signal samples for a period of one cycle. The change in energy in any of the phases of the two lines can be used to identify the faulty phase based on some threshold value. Once the faulty phase is identified the differences in magnitude and phase are utilised to identify the faulty line. For similar types of simultaneous faults on both the lines and external faults beyond the protected zone, where phasor comparison does not work, the impedance to the fault point is calculated from the estimated phasors. The computed phasors are then used to trip the circuit breakers in both lines. The proposed method for transmission-line protection includes all 11 types of shunt faults on one line and also simultaneous faults on both lines. The robustness of the proposed algorithm is tested by adding significant noise to the simulated voltage and current waveforms of a parallel transmission line. A laboratory power network simulator is used for testing the efficacy of the algorithm in a more realistic manner.

## 1 Introduction

Transmission-line protection is a key issue in power system network operation. Generally a distance protection algorithm is used to protect transmission lines under different fault conditions. Distance relaying techniques based on the measurement of the impedance at the fundamental frequency between the fault location and the relaying point have attracted widespread attention. Impedance is calculated from the phasor values of voltage and current signals retrieved at the relaying point. The value of the calculated impedance depicts whether the fault is internal or external to the protection zone. The method works satisfactorily for the protection of single-circuit lines. But when applied for the protection of parallel lines, the performance is affected by mutual coupling between two lines. In this paper, however, compensation due to mutual coupling between lines is not included as it can lead to a first-zone tripping for faults beyond the remote end of the parallel lines.

Different approaches have been attempted for protection of parallel lines by comparison of line currents of corresponding phases and positive and zero-sequence current for fault detection. Also travelling-wave based parallel-line protection has been presented [1] and as impedance an comparison between two lines has been used to detect the faulty phase [2]. As the voltage and current

signals contain the DC offset and harmonics in comparison with the fundamental component, the accuracy of the phasor estimation is affected. Fourier transforms, differential equations, waveform modelling, Kalman filters, and wavelet transforms are some of the techniques used for digital distance protection of transmission lines. Some recent papers in this area [3–7] have used only the sampled current values at the relaying point during faults for classification of fault types and distance calculations. Another pattern recognition technique based on the wavelet transform has been found to be an effective tool in monitoring and analysing power system disturbances including power-quality assessment [8] and system protection against faults [9, 10]. Although the wavelet transform provides a variable window for low- and high-frequency components in the voltage and current waveforms during faults, special threshold techniques are needed under noisy conditions. Moreover, the scalograms obtained from DWT and multiresolution signal decomposition presents only the average information of each frequency band rather than the detailed amplitude, frequency or instantaneous phase of the fundamental components that are essential for protection tasks.

In this paper a powerful time–frequency analysis known as the *S*-transform that has found applications in geosciences and power engineering [11–16] is used for the detection of faults on parallel lines and the fault distance calculations. The *S*-transform is an invertible time–frequency spectral localisation technique that combines elements of wavelet and short-time Fourier transforms. The *S*-transform uses an analysis window whose width is decreasing with frequency providing a frequency-dependent resolution. This transform may be seen as a continuous wavelet transform with a phase correction. It produces a constant relative bandwidth analysis like wavelets while it maintains a direct link with the Fourier spectrum. The *S*-transform has an advantage in that it provides

---

© The Institution of Engineering and Technology 2007

doi:10.1049/iet-gtd:20050459

Paper first received 20th October 2005 and in final revised form 21st February 2006

P.K. Dash is with The Centre for Research in Electrical, Electronics and Computer Engineering, Bhubaneswar, India

S.R. Samantaray and G. Panda are with National Institute of Technology Rourkela, India

B.K. Panigrahi is with Indian Institute of Technology Delhi, India

E-mail: sbh\_samant@yahoo.co.in

multiresolution analysis while retaining the absolute phase of each frequency. This has led to its application for detection and interpretation of events in a time series like the power-quality disturbances [12]. Further, to tackle the effects of noise and distortions, the original signal samples are passed through a Hanning window before they are processed by the  $S$ -transform.

Voltage and current signals are processed through the  $S$ -transform to yield a complex  $S$ -matrix. From the  $S$ -matrix the spectral energy is calculated for the prefault cycle and the postfault cycle. The prefault and postfault boundary is detected by using a fault detector that uses a short data window (four samples) algorithm [16]. The final indication of the fault is only given when three consecutive comparisons give the difference more than a specified threshold value. Knowing the fault instance, the change in energy that is the difference between the spectral energy of the prefault current signal for half a cycle and the postfault current signal for half a cycle is calculated. The change in energy gives an indication of the occurrence of a fault in a particular phase or more than one phase. A second part includes finding out the difference in magnitude and phase of the estimated phasors to identify the faulty phase as well as the faulty line.

The proposed approach includes three main parts. In the first, the faulty phase is detected by finding the change in energy of the prefault and postfault current signals. The second describes the identification of the faulty phase and line simultaneously from the differences in magnitude and phase of the estimated current phasors. In the third part, the impedance to the fault point is calculated in the case of similar types of fault on both the lines where the first and second approach fails substantially. The impedance trajectory is then obtained from the estimated voltage and current phasors, clearly showing the tripping characteristics of the relay for different fault conditions within the zone and also for the external faults. For providing a robust protection scheme for parallel transmission lines the change in energy and phasor estimation is carried out under noisy conditions with SNR up to 20 dB and it is observed that in most cases the  $S$ -transform provides significantly accurate results.

## 2 Time-frequency analysis of faulted power network signals

The  $S$ -transform [15] is an invertible time-frequency spectral localisation that combines elements of the short-time Fourier and wavelet transforms. The  $S$ -transform has an advantage in that it provides multiresolution analysis, retaining absolute phase of each frequency. This has led to its application for time-series analysis and pattern recognition in power networks and other engineering systems. The expression for the  $S$ -transform of a continuous signal  $x(t)$  is given as

$$S(\tau, f) = \int_{-\infty}^{\infty} x(t) \left\{ \frac{|f|}{\alpha\sqrt{2\pi}} \right\} \exp\left(\frac{-f^2(\tau-t)^2}{2\alpha^2}\right) \cdot \exp(-2\pi i f t) dt \quad (1)$$

Here  $f$  is the frequency,  $t$  is the time and  $\tau$  is a parameter that controls the position of the gaussian window on the  $t$ -axis. The factor  $\alpha$  controls the time and frequency resolution of the transform, and a lower  $\alpha$  means higher time resolution. The converse is true if a higher value of  $\alpha$  is chosen for the analysis. A suitable value of  $\alpha$ , however, lies between  $0.2 \leq \alpha \leq 1$ .

Also

$$\int_{-\infty}^{\infty} S(\tau, f) d\tau = X(f) \quad (2)$$

where  $X(f)$  is the Fourier transform of  $x(t)$ .

The discrete version of the continuous  $S$ -transform is obtained as

$$S(j, n) = \sum_{m=0}^{N-1} X(m+n) \exp\left(\frac{-2\pi^2 m^2 \alpha^2}{n^2}\right) \exp(i2\pi m j) \quad (3)$$

and  $j = 1, \dots, N-1$ ,  $n = 0, 1, \dots, N-1$ . Here  $j$  and  $n$  indicate the time samples and frequency step, respectively, and

$$X(n) = \frac{1}{N} \sum_{k=0}^{N-1} x(k) \exp(-i2\pi n k) \quad (4)$$

where  $n = 0, 1, \dots, N-1$ . Computation of  $X(m+n)$  is done in a straightforward manner from (4). The Fourier spectrum of the gaussian window at a specific  $n$  (frequency) is called a voice gaussian and for a frequency  $f_1(n_1)$  the voice is obtained as

$$S(j, n_1) = A(j, n_1) \exp(j\phi(j, n_1)) \quad (5)$$

Hence the peak value of the voice is

$$\max(S(j, n_1)) = \max(A(j, n_1)) \quad (6)$$

and

$$\phi(j, n_1) = a \tan\left\{ \frac{\text{imag}(S(j, n_1))}{\text{real}(S(j, n_1))} \right\} \quad (7)$$

The energy  $E$  of the signal is obtained from  $S$ -transform as

$$E = \{\text{abs}(S(j, n))\}^2 \quad (8)$$

From this analysis it is quite evident that not only does the  $S$ -transform localise the faulted event but also peak amplitude and phase information of the voltage and current signals can be obtained, which are important for impedance trajectory calculations. The signal energy obtained from the  $S$ -transform can be used to detect and classify the fault on the transmission line. To reduce calculations only the fundamental voice of the  $S$ -transform can be used.

$$E_{fund} = \text{abs}(S(j, n_{fund}))^2 \quad (9)$$

The succeeding Sections describe the detailed simulation study of the distance protection of parallel transmission lines using the approach presented in these formulations.

## 3 Simulation study

The model network shown in Fig. 1 has been simulated using PSCAD (EMTDC) software package. The relaying point is as shown in Fig. 1, where data is obtained for different fault conditions. The fault within the section BC is

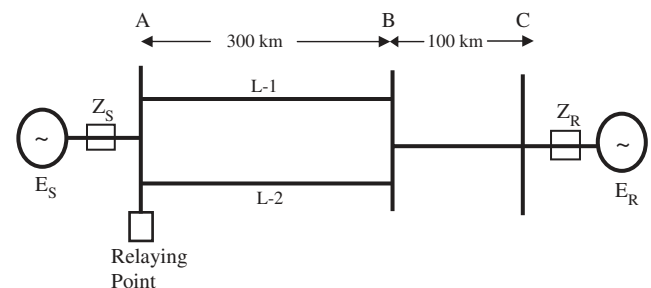


Fig. 1 Transmission line model

considered as an external fault to the relay at A. The network consists of two areas connected by two 400 kV, 300 km parallel transmission lines in section AB and an equivalent 100 km transmission line in section BC. The parameters of the transmission line are

Zero-sequence impedance of each parallel line  $Z_{L0} = 96.45 + j335.26$  ohms

Positive sequence impedance of each parallel line  $Z_{L1} = 9.78 + j110.23$  ohms

Source impedances:  $Z_S = 6 + j 28.5$  ohms,  $Z_R = 1.2 + j11.5$  ohms

Source voltages:  $E_S = 400$  kV,  $E_R = 400 \angle \delta$  kV ( $\delta =$  load angle in degrees).

For fault studies, all the three line voltage signals and six line current signals of the parallel lines are sampled at a frequency of 1.0 kHz with a base frequency of 50 Hz. The fault-detection algorithm is initiated by collecting a one-cycle sampled data window for each signal. Based on a base frequency of 50 Hz and sampling frequency of 1 kHz, one cycle of the faulted voltage or current signal contains 20 samples. For each new sample that enters the window the oldest sample is discarded, and the difference between the two is noted for three consecutive samples. If this difference exceeds a certain threshold the occurrence of a fault or an abnormal condition is assumed and the fault-calculation algorithm starts from the point of occurrence of deviation of the data sample. The data window used for fault analysis comprises a half-cycle backward and a half-cycle forward

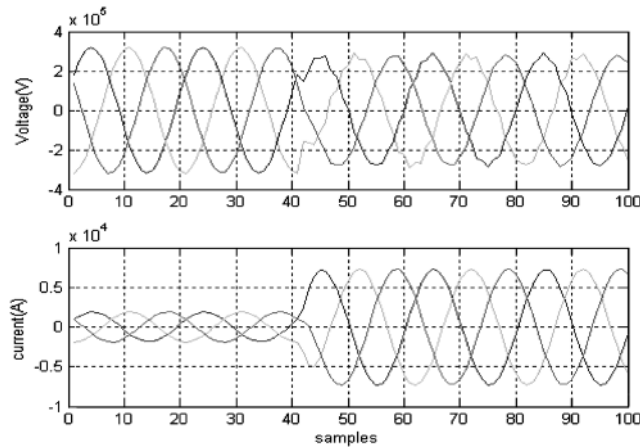


Fig. 2 Fault voltage and current signal for three-phase fault

Table 1: Change in energy for different fault conditions

| Faults                                                                                                      | Change in energy |            |            |            |            |            |
|-------------------------------------------------------------------------------------------------------------|------------------|------------|------------|------------|------------|------------|
|                                                                                                             | $cei_{a1}$       | $cei_{b1}$ | $cei_{c1}$ | $cei_{a2}$ | $cei_{b2}$ | $cei_{c2}$ |
| a-g on line 1 ( $R_f = 20$ ohm, $\delta = 30^\circ$ at 10%)                                                 | 26.40            | 1.49       | 1.80       | 2.01       | 1.09       | 1.00       |
| b-g on line 2 ( $R_f = 100$ ohm, $\delta = 45^\circ$ at 10%)                                                | 2.35             | 1.98       | 3.01       | 1.04       | 19.32      | 1.96       |
| ab-g on line 2 ( $R_f = 30$ ohm, $\delta = 60^\circ$ at 30%)                                                | 2.98             | 1.39       | 1.67       | 23.56      | 18.35      | 1.24       |
| ab on line 1 and line 2 ( $R_f = 50$ ohm, $\delta = 90^\circ$ at 50%)                                       | 22.12            | 18.36      | 0.02       | 20.36      | 19.38      | 0.01       |
| bc on line 2 ( $R_f = 120$ ohm, $\delta = 45^\circ$ at 70%)                                                 | 0.01             | 0.14       | 0.18       | 0.03       | 16.89      | 15.25      |
| abc on line 2 ( $R_f = 150$ ohm, $\delta = 30^\circ$ at 70%)                                                | 1.23             | 0.25       | 1.05       | 12.49      | 16.24      | 14.89      |
| abcg on line 1 and line 2 ( $R_f = 200$ ohm, $\delta = 60^\circ$ at 90%)                                    | 10.98            | 11.21      | 13.15      | 11.69      | 10.98      | 14.25      |
| abcg on line 1 ( $R_f = 150$ ohm, $\delta = 90^\circ$ at 70%) with source impedance changed (increased 10%) | 9.23             | 8.25       | 7.26       | 0.21       | 0.65       | 0.98       |
| abcg on line 2 ( $R_f = 150$ ohm at 70%) with source impedance changed (increased 30%)                      | 0.84             | 0.24       | 0.58       | 8.36       | 10.98      | 9.99       |

from the detection of an abnormality. The  $S$ -transform calculates the time-frequency contours from which the peak amplitude and phase of the voltage and current signals along with the change in energy values are derived. The fault voltage and current signals for a three-phase fault at 50% of line section AB are shown in Fig. 2.

## 4 Proposed method

### 4.1 Faulty phase selection based on change in energy

The fault current signal is considered for faulty phase detection for different types of faults on one line or both the lines. From the  $S$ -transform matrix the energy content of the respective current signals is calculated. A change in energy of the signal is calculated by deducting the  $S$ -transform energy content of the signal after a half cycle of fault inception from the energy content of the signal half a cycle before the fault inception. The change in energy of the  $S$ -transform of the current signal clearly indicates the faulty phase from the unfaulted one. Changes in energy for the three phases of line 1 are  $cei_{a1}$ ,  $cei_{b1}$ ,  $cei_{c1}$  and  $cei_{a2}$ ,  $cei_{b2}$ ,  $cei_{c2}$  are changes in energy for the three phases for line 2. Tables 1 and 2 depict the changes in energy for various types of faults for different locations, various fault resistances, source impedances, and different inception angles.

Changes in the signal energy of the  $S$ -transform contour are obtained as

$$ce = E_f - E_A = \{abs(h_f)\}^2 - \{abs(h_n)\}^2 \quad (10)$$

where  $h_f$  is the  $S$ -matrix coefficient for postfault current and  $h_n$  is the  $S$ -matrix coefficient for prefault current.

The relay is set with all the six values of change in energy with a threshold value and the calculated change in energy is compared with that of the threshold value and the faulty phase is identified when the calculated value exceeds the threshold value.

From Table 1 it is clearly seen that the faulty phase has maximum change in energy compared with unfaulted phases. For an a-g fault with fault resistance  $R_f = 20$  ohms, inception angle  $\delta = 30^\circ$  at 10% of the transmission line,  $cei_{a1} = 26.40$  while  $cei_{b1} = 1.49$ ,  $cei_{c1} = 1.80$ ,  $cei_{a2} = 2.01$ ,  $cei_{b2} = 1.09$  and  $cei_{c2} = 1.00$ , which clearly shows that there is an a-g (line-to-ground fault on line 1). The threshold value chosen here is 5.0 above which the phase is identified as faulty.

The change in energy values for different types of fault has been found using various operating conditions including

**Table 2: Change in energy for different fault conditions with SNR 20 dB**

| Faults                                                                                                      | Change in energy |               |               |               |               |               |
|-------------------------------------------------------------------------------------------------------------|------------------|---------------|---------------|---------------|---------------|---------------|
|                                                                                                             | $ce_{i_{a1}}$    | $ce_{i_{b1}}$ | $ce_{i_{c1}}$ | $ce_{i_{a2}}$ | $ce_{i_{b2}}$ | $ce_{i_{c2}}$ |
| a–g on line 1 ( $R_f = 20$ ohm, $\delta = 30^\circ$ at 10%)                                                 | 28.69            | 2.65          | 1.00          | 2.11          | 1.12          | 1.05          |
| b–g on line 2 ( $R_f = 100$ ohm, $\delta = 45^\circ$ at 10%)                                                | 2.45             | 1.92          | 2.01          | 1.23          | 20.12         | 1.69          |
| ab–g on line 2 ( $R_f = 30$ ohm, $\delta = 60^\circ$ at 30%)                                                | 3.01             | 1.56          | 1.74          | 25.64         | 19.68         | 1.54          |
| ab on line 1 and line 2 ( $R_f = 50$ ohm, $\delta = 90^\circ$ at 50%)                                       | 23.12            | 20.02         | 0.12          | 21.32         | 19.36         | 0.02          |
| bc on line 2 ( $R_f = 120$ ohm, $\delta = 45^\circ$ at 70%)                                                 | 0.11             | 0.15          | 0.28          | 0.18          | 17.36         | 18.65         |
| abc on line 2 ( $R_f = 150$ ohm, $\delta = 30^\circ$ at 70%)                                                | 1.35             | 0.68          | 1.21          | 13.56         | 17.36         | 15.64         |
| abcg on line 1 and line 2 ( $R_f = 200$ ohm, $\delta = 60^\circ$ at 90%)                                    | 11.23            | 12.36         | 14.32         | 12.36         | 12.65         | 16.28         |
| abcg on line 1 ( $R_f = 150$ ohm, $\delta = 90^\circ$ at 70%) with source impedance changed (increased 10%) | 10.36            | 9.36          | 8.64          | 0.25          | 0.98          | 1.02          |
| abcg on line 2 ( $R_f = 150$ ohm at 70%) with source impedance changed (increased 30%)                      | 0.98             | 0.25          | 0.87          | 9.36          | 11.54         | 11.23         |

different fault resistances, inception angles, source impedances, and different locations with all 11 types of shunt fault and is shown in Tables 1 and 2. The proposed method is also tested under noisy conditions when a white gaussian noise of SNR = 20 dB is added to the voltage or current signals. A higher value of change in energy for a particular phase indicates the occurrence of the fault in that phase. Table 2 shows the calculated energy values under noisy conditions and the results given in this Table shows that the proposed method provides satisfactory results under noisy conditions.

#### 4.2 Faulty-line selection based on phasor comparison

After detecting the disturbance on the faulty phase from the change in energy the corresponding faulty line can be detected and a trip signal can be sent to the circuit breaker by calculating the difference in magnitude of the faulted current signal from the estimated phasors. The amplitude and phase of the fault current and voltage signal are calculated from the  $S$ -transform matrix. Since the  $S$ -matrix is complex the peak amplitude of the signal is found as

$$\text{amplitude} = \max(\text{abs}(S)) \quad (11)$$

From the  $S$ -matrix the frequency–amplitude relationship is obtained showing clearly the frequency at which the maximum amplitude of the fault current and voltage signals occurs. The instantaneous phase of the signal is found at the exact frequency voice where the amplitude is maximum as

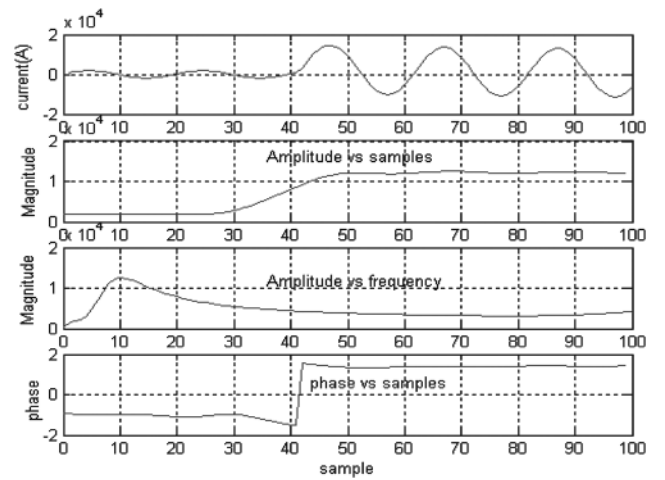
$$ph = a \tan(\text{imag}(S)/\text{real}(S)) \quad (12)$$

Figure 3–6 show the magnitude and phase of the fault current and voltage for a single line-to-ground fault (a–g) at 10% of the line length without noise and with noise (SNR = 20 dB), respectively. From the Figures it is found that the peak magnitudes and phase angle of the voltage and current signals are hardly influenced by the presence of 20 dB noise. After computing the peak amplitude and phase angle of voltage and current signals during faults it is necessary to find the tripping signals for the circuit breakers for line 1 and line 2 of the parallel transmission lines, respectively.

The differences in the magnitude and phase of the current signals in the two parallel transmission lines are obtained as

$$I_{magdiff} = I_{mag1} - I_{mag2} \quad (13)$$

$$I_{phdiff} = I_{ph1} - I_{ph2} \quad (14)$$



**Fig. 3** Magnitude and phase for current at a–g fault at 10%,  $R_f = 20$  ohm

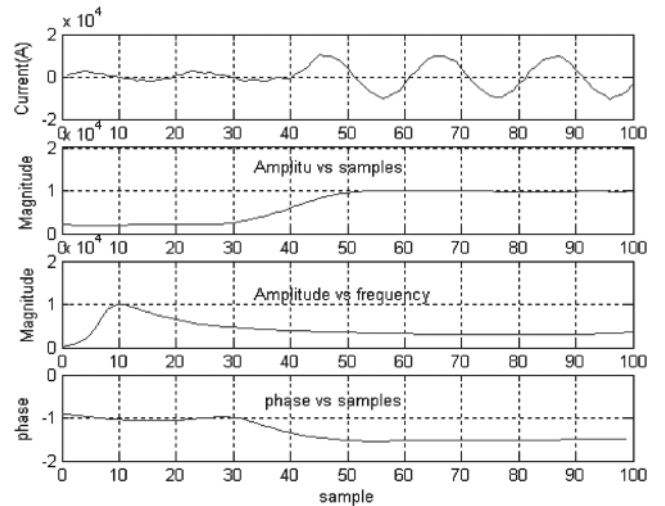


**Fig. 4** Magnitude and phase for current at a–g fault at 10%,  $R_f = 20$  ohm with SNR 20 dB

where  $I_{mag1}$  and  $I_{mag2}$  are the estimated magnitude of fault current signal for line 1 and line 2, respectively. Similarly  $I_{ph1}$  and  $I_{ph2}$  are the estimated phase of fault current signal of line 1 and line 2, respectively. Likewise, the difference in magnitude and phase of the current signal for other phases of the lines can be calculated. For positive values of  $I_{magdiff}$

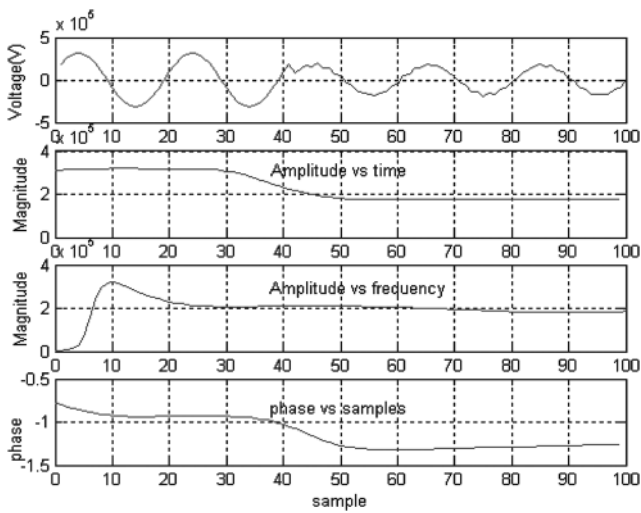


**Fig. 5** Magnitude and phase for voltage at a-g fault at 10%,  $R_f = 20$  ohm

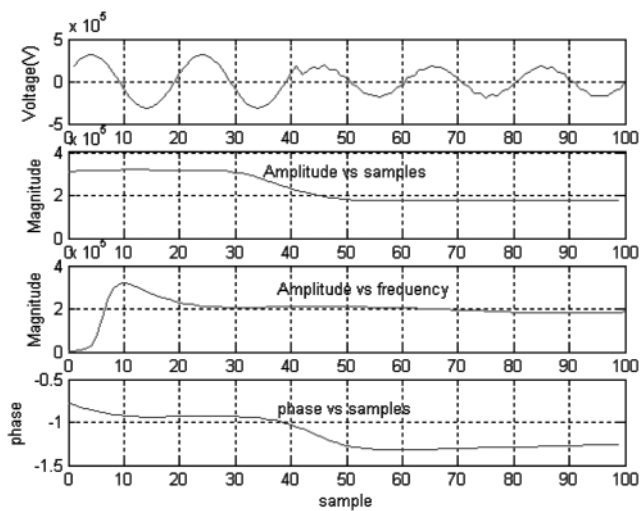


**Fig. 6** Magnitude and phase for voltage at a-g fault at 10%,  $R_f = 20$  ohms with SNR 20 dB

above a threshold value the relay trips the circuit breaker of line 1, and for a negative value below the threshold the relay trips the circuit breaker of line 2. Similarly, a trip signal for the circuit breakers in lines 1 and 2 can be generated.

Figure 7 depicts the line-ground fault (a-g) on line 1, where  $I_{magdiff}$  increases from the 0 to 6000. The threshold value is chosen as  $\pm 1000$  taking into account all operating conditions of fault resistance, source impedance, fault location and inception angles. When  $I_{magdiff}$  exceeds the threshold value of +1000 the relay trips line 1 and when the value is -1000 the relay trips the line 2 circuit breaker. Figure 8 shows  $I_{magdiff}$  for a line-ground fault (a-g) at 30% of line 1 and a b-g fault at 30% of line 2 with 100 ohms fault resistance for section AB. Figure 9 shows the value of  $I_{magdiff}$  for a line-line-ground fault (ab-g) at 50% of line 1 with 150 and 200 ohms fault resistance for section AB, respectively. Similarly, Fig. 10 shows the  $I_{magdiff}$  for a line-ground fault (a-g) at 90% of line 1 with 200 ohm fault resistance for section AB. Figures 11 and 12 show the  $I_{magdiff}$  for a line-ground fault (a-g) at 30% of line 1 and ab-g fault at 80% of line 2 with 20 ohms fault resistance for section AB and for line-ground fault (a-g) at 30% of line 1 with 50 ohms fault resistance for section AB with SNR 20 dB, respectively. These results clearly identify the faulty

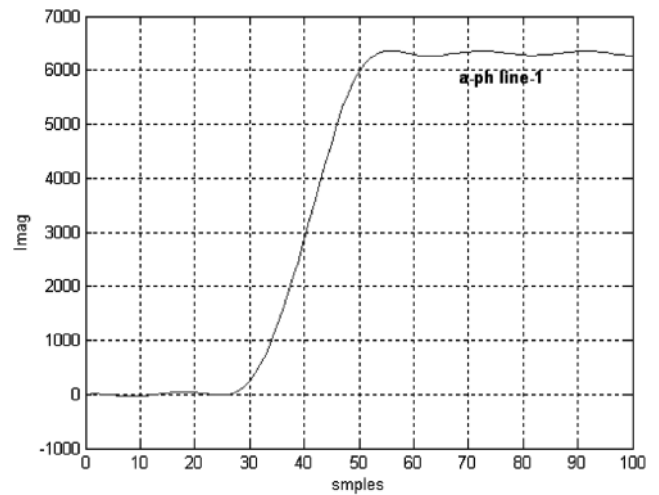


**Fig. 7**  $I_{magdiff}$  for line-ground fault (a-g) at 10% of the line 1 with 50 ohms fault resistance for section AB

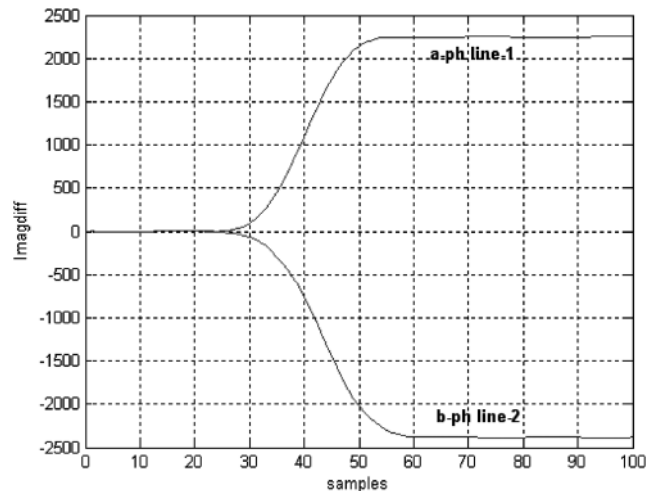


**Fig. 8**  $I_{magdiff}$  for line-ground fault (a-g) at 30% of the line 1 and b-g fault at 30% of the line 2 with 100 ohms fault resistance for section AB

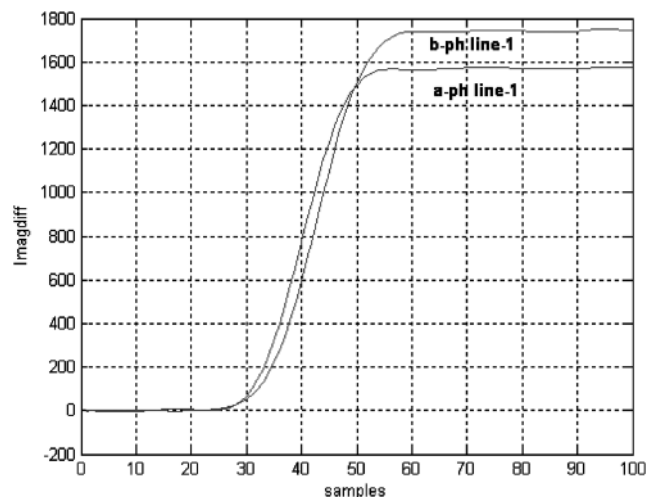


**Fig. 9**  $I_{magdiff}$  for line-line-ground fault (ab-g) at 50% of the line 1 with 150 ohms fault resistance for section AB

phase as well as the line involved under widely varying operating conditions.

Figures 13 and 14 show  $I_{phdiff}$  for a line-ground fault (a-g) at 30% of line 1 with 20 ohms fault resistance for the

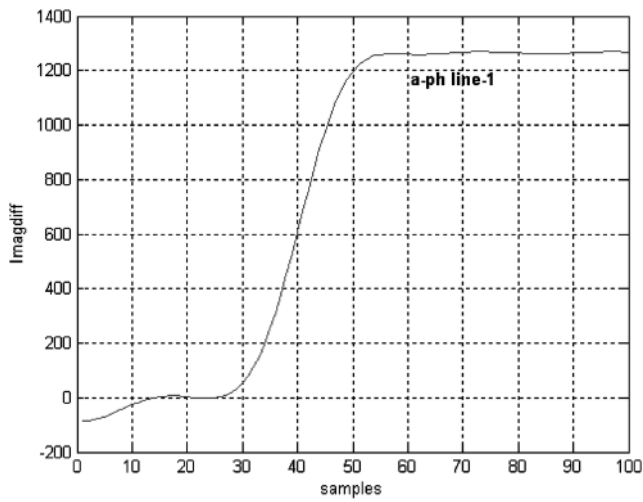


**Fig. 10**  $I_{magdiff}$  for line-ground fault (a-g) at 90% of the line 1 with 200 ohms fault resistance for section AB

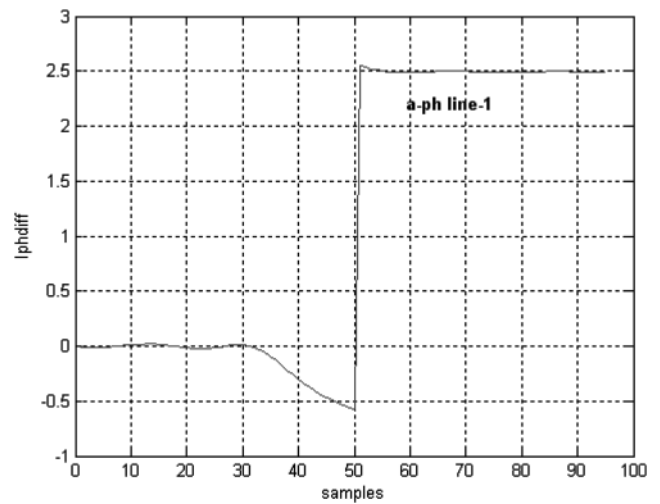


**Fig. 13**  $I_{phdiff}$  for line-ground fault (a-g) at 30% of the line 1 with 20 ohms fault resistance for section AB

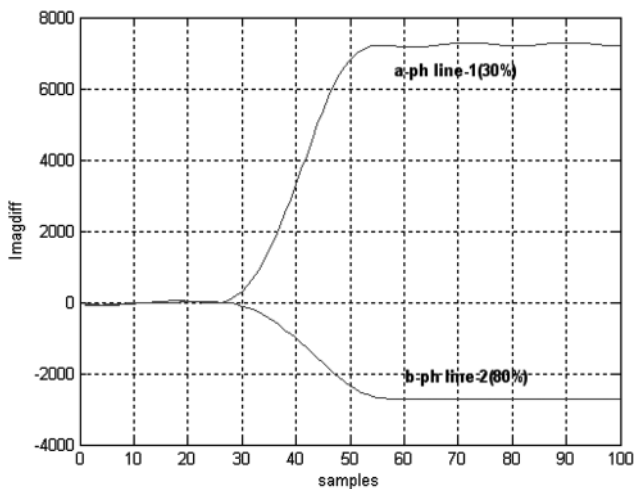


**Fig. 11**  $I_{magdiff}$  for line-ground fault (a-g) at 30% of the line 1 and b-g fault at 80% of line 2 with 20 ohms fault resistance for section AB

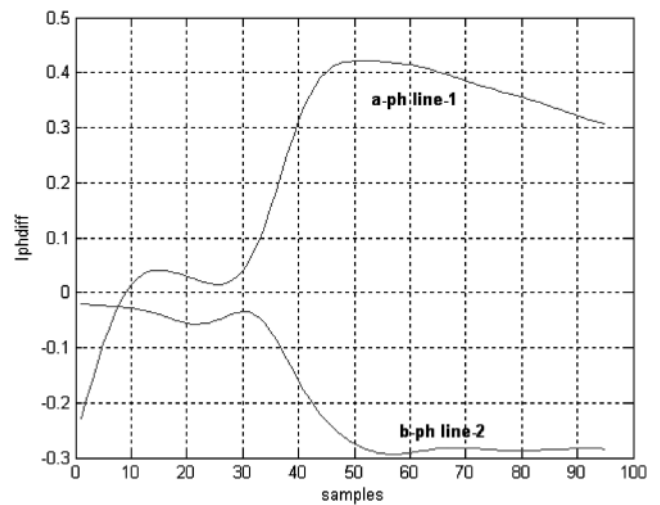


**Fig. 14**  $I_{phdiff}$  for line-ground fault (a-g) on line 1 and b-g fault on line 2 at 90% of lines with 200 ohms fault resistance for section AB

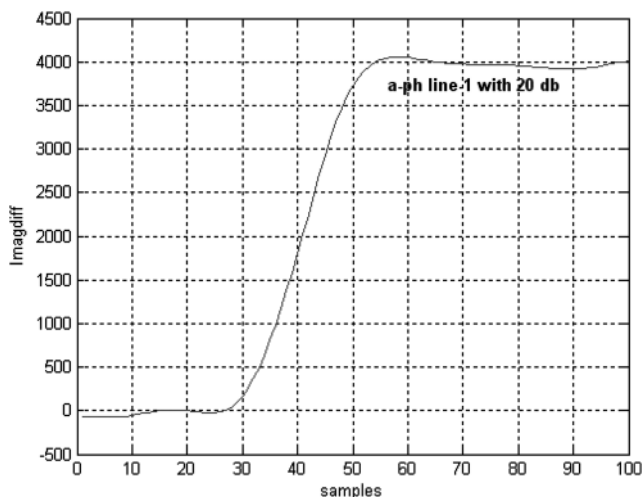


**Fig. 12**  $I_{magdiff}$  for line-ground fault (a-g) at 30% of the line 1 with 50 ohms fault resistance for section AB with SNR 20 dB

section AB and for a line-ground fault (a-g) on line 1 and b-g fault on line 2 at 90% of lines with 200 ohms fault resistance for the same section. The threshold limits for

$I_{phdiff}$  are chosen as  $I_{phdiff1} = +0.25$ ,  $I_{phdiff2} = -0.25$ , taking all operating conditions into consideration.

### 4.3 Impedance trajectory

The magnitude and phase difference of the fault voltage and current in different phases works successfully in case of different types of fault on either of lines. But for similar types of fault on both lines simultaneously the method doesn't work. This problem arises in the case of an a-g fault on line 1 and on line 2, an ab-g fault on line 1 and on line 2, an a-b fault on line 1 and line 2, and an abc-g fault on line 1 and on line 2 simultaneously. In these cases the difference in magnitude and phase does not provide adequate information regarding the faulted condition as the difference may give values nearly zero or much below the threshold value set for the relay to respond to the magnitude difference in identifying the faulty phase as well as the faulty line. The problem can only be solved by calculating the impedance of the line to the fault point. The impedance trajectory provides the information as to whether the line is under a fault condition or is healthy and accordingly the circuit breaker is tripped if the impedance trajectory enters the tripping zone of the relay.

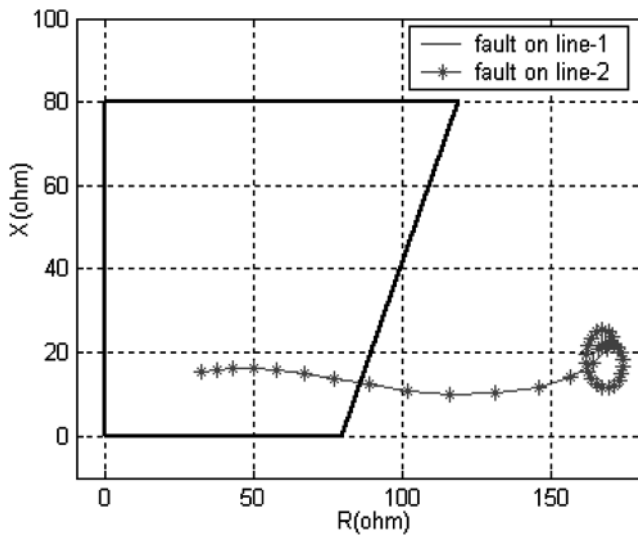


**Fig. 15**  $R$ - $X$  plot for  $a$ - $g$  fault on line 1 and line 2 at 10% of both the line with 10 ohms fault resistance

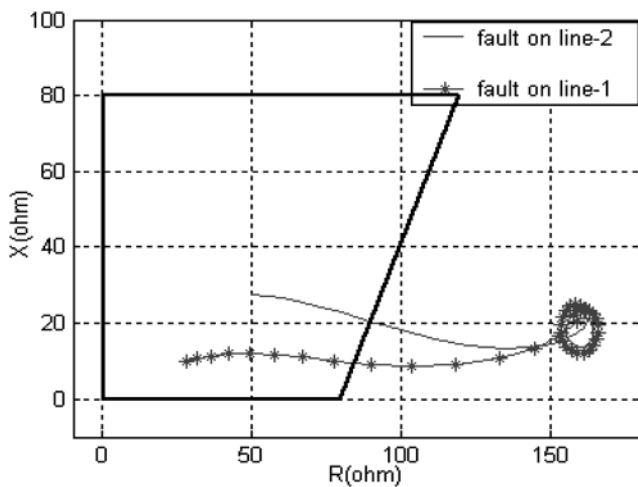


**Fig. 16**  $R$ - $X$  plot for  $b$ - $g$  fault on line 1 at 20% of line 1 and  $b$ - $g$  fault at 50% of line 2 with 10 ohms fault resistance

**4.3.1 Fault within protected zone; impedance seen by relay at 'A':** The impedance is calculated from the methods depicted in the Appendix (Section 7) and from the impedance trajectory it is clearly seen that in case of faults the trajectory comes within the relay operating zone. Figure 15 shows the  $R$ - $X$  plot for  $a$ - $g$  (line-ground) fault on lines 1 and 2 simultaneously with a fault resistance of 10 ohms, and the trajectory enters the tripping zone within eight samples after the fault detection. It is found that the  $R$ - $X$  plot for the  $a$ - $g$  fault on line 1 and the  $R$ - $X$  plot for the  $a$ - $g$  fault on line 2 overlap each other as the operating conditions for both the lines remain same. Similarly, Fig. 16 depicts the  $R$ - $X$  plot for a  $b$ - $g$  (line-ground) fault on line 1 at 20% of line length and a  $b$ - $g$  fault on line 2 at 50% of line length with 10 ohms fault resistance.

The algorithm has been tested for various operating conditions with 0–200 ohms fault resistance, variable source impedance (up to 130%), and various inception angles and at various locations for all the 11 types of shunt faults. Also the  $R$ - $X$  trajectory enters the tripping characteristics within eight samples after the fault on a particular phase is detected and thus the total fault tripping time is less than 18 samples (less than one cycle), which proves the speed of the proposed method. The speed of the proposed algorithm

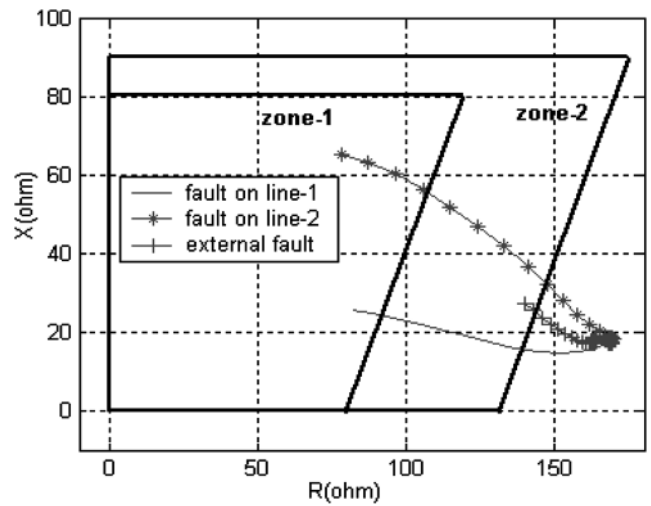


**Fig. 17**  $R$ - $X$  plot for  $a$ - $b$  fault on line 1, line 2 and line 3

can be further improved if the identification of the faulty phase can be achieved in less than half a cycle, in a quarter of a cycle for instance.

#### 4.3.2 External faults; impedance seen by the relay at 'A':

For external faults  $I_{magdiff}$  and  $I_{phdiff}$  are almost zero for the corresponding phase. Thus determination of the impedance trajectory provides the necessary protection to the line. The fault in the section BC is considered as an external fault for the relay at A. Figure 17 shows the impedance trajectory for  $a$ - $b$  fault (line-line) at 20% on line 1 (AB), 70% on line 2 (AB) and at 20% in section BC with a fault resistance of 50 ohms in all cases. From Fig. 17 it is clearly seen that for a fault on line 1 (AB) and a fault on line 2 (AB) the impedance trajectory enters into the tripping zone of the relay within eight samples from the detection of fault and less than one cycle from the inception of the fault. The impedance trajectory for the faults within section BC (20% of line BC) doesn't come inside the zone-1 tripping area of relay A, but it enters the zone-2 tripping area of the relay at A. This indicates that for external faults the relay at A provides backup protection.

#### 4.4 Results from laboratory power network simulator

The proposed algorithm has been tested on a physical transmission-line model. The transmission line consists of two parallel lines (section AB), each of 150 km  $\pi$ -sections and another 100 km  $\pi$ -section (section BC). The line is charged with 400 V, 5 kVA synchronous machines at one end and 400 V at the load end. The three-phase voltage and current are stepped down at the relaying end with a potential transformer of 400/10 V and current transformer of 15/5 A, respectively. Data was collected using a PCL-208 data acquisition card which uses 12-bit successive-approximation technique for A/D conversion. The card is installed on a PC (P-IV) with a driver software routine written in C++. It has six I/O channels with input voltage range of  $\pm 5$  V. Data was collected with a sampling frequency of 1.0 kHz.

The results are shown in Figs. 18–22. Figure 18 shows  $I_{magdiff}$  for a line-ground (L-G) fault at 50 km of line 1 and Fig. 19 shows the  $I_{magdiff}$  for a line-line (L-L) fault at 100 km on line 1 and line 2, respectively. The phase difference for the same fault is shown in Fig. 20. The threshold for  $I_{magdiff}$  is  $\pm 3.0$  and for  $I_{phdiff}$  is  $\pm 0.25$ . The line-ground fault impedance trajectory at 50 km on line 1 is

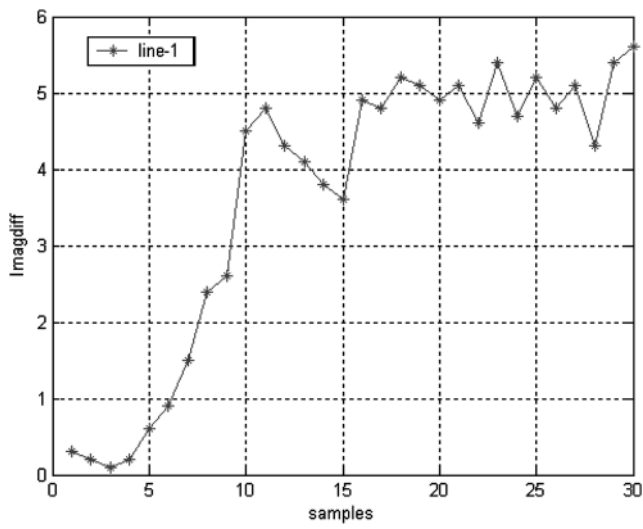


Fig. 18  $I_{magdiff}$  for L-G fault at 50 km on line 1

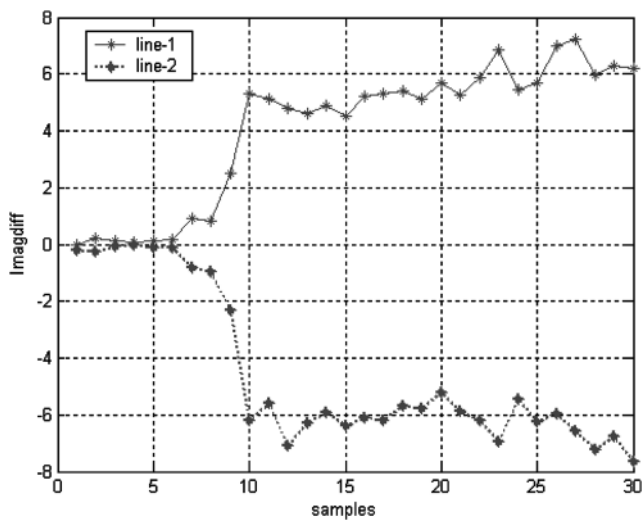


Fig. 19  $I_{magdiff}$  for L-L fault at 100 km on line 1 and line 2

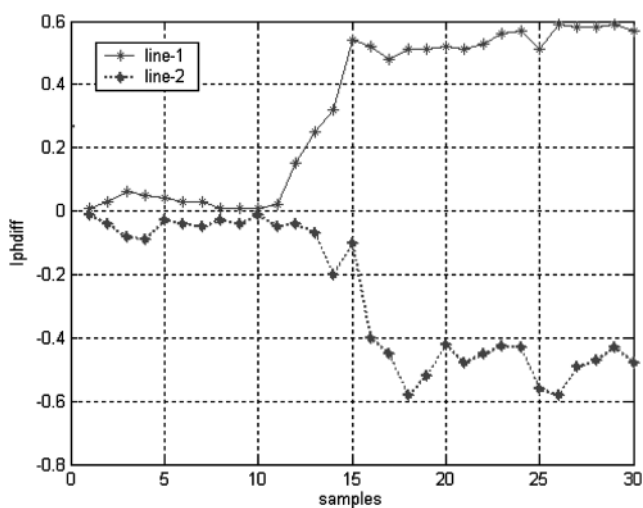


Fig. 20  $I_{phdiff}$  for L-L fault at 100 km on line 1 and line 2

shown in Fig. 21. The impedance trajectory for LL-G fault on both lines at 100 km is depicted in Fig. 22. It is found that the trajectory enters into the relay operating zone

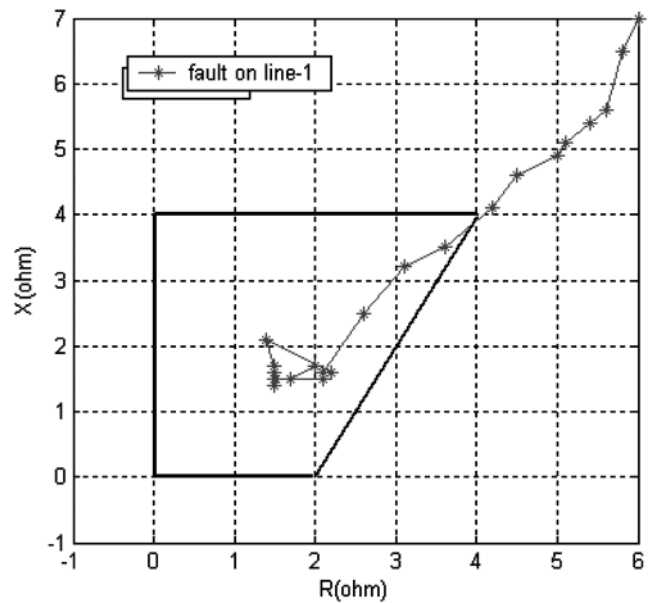


Fig. 21  $R-X$  plot for L-G fault at 50 km on line 1

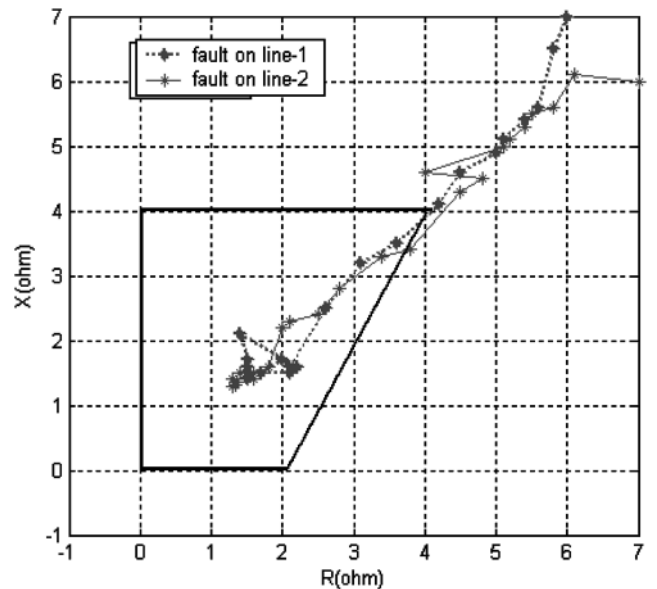


Fig. 22  $R-X$  plot for LL-G fault at 100 km on line 1 and line 2

within eight samples of the fault detection (18 samples after the fault inception). As the operating voltage range is 400 V, the relay zone and threshold values are selected accordingly. These results show that the proposed method works satisfactorily in laboratory environments.

## 5 Conclusions

A new distance relaying scheme using the  $S$ -transform for protection of parallel transmission line has been presented. The faulty phase on either of the lines is detected by finding out the change in energy for the corresponding phase. After the faulty phase detection the corresponding faulty line is identified by finding the magnitude and phase difference of the estimated current phasor. In the case of similar types of fault on both the lines simultaneously and external faults on the line, the difference in magnitude and phase cannot be used to identify the faulty line. In that case the impedance to the fault point is calculated from the estimated phasors of the faulted current and voltage signals. The relay trips the



circuit breaker when impedance trajectory enters the tripping zone of the relay. Thus the proposed method provides protection of parallel lines which includes all 11 types of shunt faults on both the lines with different operating conditions. The algorithm detects the fault and identifies the line within one cycle of inception of fault and provides accurate results even in the presence of white noise of low SNR values. Further, the  $S$ -transform localises the time of occurrence of the fault while providing an accurate calculation of amplitude and phase of fundamental voltage and current signals required for the computation of the impedance trajectory. The delayed fault clearance problem due to overloading is being studied and the sensitivity of the  $S$ -transform to this problem will be reported later.

## 6 References

- 1 Boolean, M.H.J.: 'Travelling wave based protection of double circuit lines', *Proc. IEE C*, 1993, **140**, (1), pp. 37–47
- 2 Issa, M.M., and Masoud, M.: 'A novel digital distance relaying technique for transmission line protection', *IEEE Trans. Power Deliv.*, 2001, **16**, pp. 380–384
- 3 Youssef, O.A.S.: 'New algorithms for phase selection based on wavelet transforms', *IEEE Trans. Power Deliv.*, 2002, **17**, pp. 908–914
- 4 Youssef, O.A.S.: 'Online applications of wavelet transform to power system relaying', *IEEE Trans. Power Deliv.*, 2003, **18**, (4), pp. 1158–1165
- 5 Youssef, O.A.S.: 'Combined fuzzy-logic wavelet-based fault classification for power system relaying', *IEEE Trans. Power Deliv.*, 2004, **19**, (2), pp. 582–589
- 6 Gilany, M.I., Malik, O.P., and Hope, G.S.: 'A digital technique for parallel transmission lines using a single relay at each end', *IEEE Trans. Power Deliv.*, 1992, **7**, pp. 118–123
- 7 Jongepier, A.G., and van der Sluis, L.: 'Adaptive distance protection of a double circuit line', *IEEE Trans. Power Deliv.*, 1994, **9**, pp. 1289–1295
- 8 Gauda, M., Salama, M.A., Sultam, M.R., and Chikhani A., Y.: 'Power quality detection and classification using wavelet multi-resolution signal decomposition', *IEEE Trans. Power Deliv.*, 1999, **14**, pp. 1469–1476
- 9 Osman, A.H., and Malik, O.P.: 'Transmission line protection based on wavelet transform', *IEEE Trans. Power Deliv.*, 2004, **19**, (2), pp. 515–523
- 10 Chanda, D., Kishore, N.K., and Sinha, A.K.: 'A wavelet multi-resolution analysis for location of faults on transmission lines', *Electr. Power Energy Syst.*, 2003, **25**, pp. 59–69
- 11 Mansinha, L., Stockwell, R.G., and Lowe, R.P.: 'Pattern analysis with two-dimensional spectral localization: Application of two-dimensional  $S$ -transforms', *Physica A*, 1997, **239**, pp. 286–295
- 12 Dash, P.K., Panigrahi, B.K., and Panda, G.: 'Power quality analysis using  $S$ -transform', *IEEE Trans. Power Deliv.*, 2003, **18**, pp. 406–411
- 13 Livanos, G., Ranganathan, N., and Jiang, J.: 'Heart sound analysis using the  $S$ -transform', *IEEE Comp. Cardiol.*, 2000, **27**, pp. 587–590
- 14 Pinnegar, C.R., and Mansinha, L.: 'The  $S$ -transform with windows of arbitrary and varying window', *Geophysics*, 2003, **68**, pp. 381–385
- 15 Stockwell, R.G., Mansinha, L., and Lowe, R.P.: 'Localization of complex spectrum: the  $S$ -transform', *J. Assoc. Expl. Geophys.*, 1996, **XVII**, (3), pp. 99–114
- 16 Mann, B.J., and Morrison, I.F.: 'Relaying a three phase transmission line with a digital computer', *IEEE Trans. Power Appar. Syst.*, 1971, **PAS 90**, (2), pp. 742–750

## 7 Appendix

After the phasor calculation, impedance to the fault point is calculated by using the phasor information. The  $R-X$  trajectory is found from the impedance information which clearly shows how the trajectory enters within the relay operating zone for different fault conditions to protect the line and does not enter the relay zone in case of an unfaulted condition. The impedance is calculated as follows:

- For phase-earth fault

$$Z_{ph} = \frac{V_{ph}}{I_{ph}(1) + I_{ph}(2) + KI_{ph}(0)} \quad (15)$$

where  $V_{ph}$  is the estimated amplitude of the phase voltage, and  $I_{ph}(1)$ ,  $I_{ph}(2)$ ,  $I_{ph}(0)$  are the estimated amplitudes of the positive, negative, and zero sequence currents, respectively.

- For phase-phase fault

$$Z_{ab} = \frac{V_a - V_b}{I_a - I_b} \quad (16)$$

where  $V_a$  and  $V_b$  are estimated voltage amplitudes and  $I_a$  and  $I_b$  are estimated current amplitudes.